DOI 10.24425/aee.2025.155961

Inter-turn short-circuit fault diagnosis of high-voltage line-start permanent magnet synchronous motor based on improved wavelet packet energy analysis

CUNXIANG YANG[1], SHIZHENG ZHANG[1], YUNZHUANG WANG[1], HONGBO QIU[2]✉, HEWEI ZHAO[1]

[1] *College of Building Environment Engineering, Zhengzhou University of Light Industry Zhengzhou city, Henan, China*

[2] *College of Electric and Information Engineering, Zhengzhou University of Light Industry Zhengzhou city, Henan, China*

e-mail: yangzzha@zzuli.edu.cn, 1024244235@qq.com, {332313030896/✉ qiuhongbo/332313030900}@zzuli.edu.cn

(Received: 28.04.2025, revised: 03.11.2025)

Abstract: High-voltage line-start permanent magnet synchronous motors (HVLSPMSMs) are prone to inter-turn short-circuit faults, which not only result in a significant increase in current but also exacerbate motor vibration. To accurately identify the frequency-domain fault characteristics of the motor under inter-turn short-circuit conditions, an improved wavelet packet energy gain ratio analysis method is proposed. Firstly, a two-dimensional transient finite element simulation model is established, and the validity of the model is verified through experimental data. On this basis, the inter-turn short-circuit fault state of the motor is further analyzed, and the corresponding fault signals are extracted. Secondly, the improved wavelet packet transform (IWPT) is applied to analyze the fault current and vibration signals. By combining the energy gain ratio, fast Fourier transform (FFT) is conducted on the sensitive wavelet packet coefficient nodes to extract the fault characteristics of the current and vibration signals by comparing the frequencies before and after the fault occurrence. Finally, a comparison with traditional wavelet packet analysis demonstrates the reliability and accuracy of the proposed method.

Key words: energy gain ratio, fast Fourier transform, high-voltage line-start permanent magnet synchronous motor, improved wavelet packet transform, inter-turn short circuit faults

1. Introduction

Permanent magnet motors are characterized by high power factor, high efficiency, and ease of maintenance. As a result, the application of permanent magnet motors has become increasingly widespread, particularly for self-starting permanent magnet synchronous motors (PMSMs), which combine the advantages of simple operation and maintenance similar to induction motors, while offering high efficiency [1]. In industry, the widespread adoption of permanent magnet motors to replace induction motors has significantly reduced energy consumption in industrial production. High-voltage motors are used to drive various mechanical systems and are a primary power source for industrial production and mining, as well as prime movers in industries like power generation, mechanical, petrochemical, and metallurgy. However, high-voltage line-start permanent magnet synchronous motors (HVLSPMSMs), which operate in complex environments, are prone to various faults, with common issues including stator inter-turn short circuits, permanent magnet demagnetization, and rotor eccentricity [2]. Among these, inter-turn short circuit faults occur frequently [3], and the occurrence of such faults not only affects the vibration performance of the motor, but if undetected in the early stages, can lead to continuous overheating and damage to the motor, even posing risks to personal safety. Therefore, fault detection of inter-turn short circuits in motors is of significant importance.

Researchers both domestically and internationally have conducted extensive studies on fault detection for permanent magnet synchronous motors. The current methods for fault detection in motors include model-based analysis, signal processing, and deep learning approaches [4–6]. With the increasing number of industrial devices in use, the demand for equipment fault diagnosis has also grown. More researchers are focusing on analyzing the status information of equipment from measurement data. Traditional signal processing methods, such as fast Fourier transform (FFT), have been widely applied and proven effective in machine diagnostics. For example, in Reference [7], FFT is used to analyze current and vibration signals under fault conditions, and the fault features under inter-turn short circuit are extracted from the frequency spectrum changes. In Reference [8], FFT is applied to torque signal analysis, extracting fault features related to inter-turn short circuits in motors. However, due to the complex operating conditions of motors and their susceptibility to noise, the precision of direct Fourier transform analysis is relatively low.

For nonlinear signals like those from permanent magnet synchronous motor current and vibration, wavelet transforms, such as continuous wavelet transform (CWT) and discrete wavelet transform (DWT), have become powerful tools for signal analysis. They decompose the signals into different scales and positions, providing a multi-resolution time-frequency representation that aids in fault feature identification. Reference [9] uses DWT to filter stator current to improve precision for fault detection. Reference [10] applies wavelet decomposition of stator current and calculates the energy at each node, comparing the energy variations before and after the fault for fault detection. However, wavelet transforms also have limitations, they focus on the low-frequency components of the signal and overlook the high-frequency parts [11]. To address this, wavelet packet transform (WPT) was introduced. WPT analyzes not only the low-frequency but also the high-frequency components of the signal, enabling more effective use of the signal [12]. Reference [13] analyzes the torque under different short-circuit turns in the motor, extracts fault features, and inputs them into an artificial neural network for fault recognition. However, due to the characteristics of wavelet filters and the algorithms in WPT, frequency aliasing problems are

inevitable. Improved wavelet packet transform (IWPT) was developed to overcome these issues. By eliminating the effects caused by filter characteristics, interval sampling, and interpolation, IWPT effectively resolves the frequency aliasing problem.

Currently, research on fault diagnosis primarily focuses on asynchronous motors and permanent magnet synchronous motors. However, research on fault diagnosis for HVLSPMSMs is noticeably insufficient. Moreover, due to the complex operating conditions of HVLSPMSMs, the fault characteristics of the signals are more susceptible to interference from environmental factors and noise, making detection more challenging compared to conventional motors. Therefore, this paper proposes a fault feature extraction method based on the IWPT analysis combined with energy gain ratio analysis, using both current and vibration signals. IWPT is applied for multi-layer decomposition of the current and vibration signals, eliminating frequency aliasing, and achieving multi-resolution analysis. Fault features are reflected in the wavelet packet coefficients, which are transformed into energy features. Based on this, the energy gain ratio of the wavelet packet is analyzed, and by examining the changes in the wavelet packet coefficients in the frequency domain, the primary fault characteristics of the motor current and vibration signals post-fault are extracted.

2. Finite element modeling and fault state analysis of HVLSPMSM

2.1. Establishment of the finite element model

A 10 kV, 630 kW HVLSPMSM is analyzed in this paper, with the motor parameters presented in Table 1. Based on the actual structure of the prototype, a two-dimensional model of the motor is established. The structure and mesh division of the motor results are shown in Fig. 1. To enhance solution accuracy, fine meshes are applied in regions with high physical variation rates, while coarse meshes are used in regions with low variation rates [14], thereby optimizing computation time. The total number of mesh elements in the model is 65 812.

Table 1. The HVLSPMSM basic parameters

Parameters (unit)	Value	Parameters (unit)	Value
Rated power (kW)	630	Stator inner diameter (mm)	600
Frequency (Hz)	50	Stator outer diameter (mm)	880
Rated voltage (kV)	10	Rotor inner diameter (mm)	360
Rated speed (rpm)	750	Rotor outer diameter (mm)	595
Slot number	36	Stator length (mm)	275
Polar logarithm	4	Length of air-gap (mm)	2.5
Number of stator slots	72	Parallel branches	1
Number of rotor slots	56	Conductors per slot	14
Number of strands	1	Type of circuit	Y

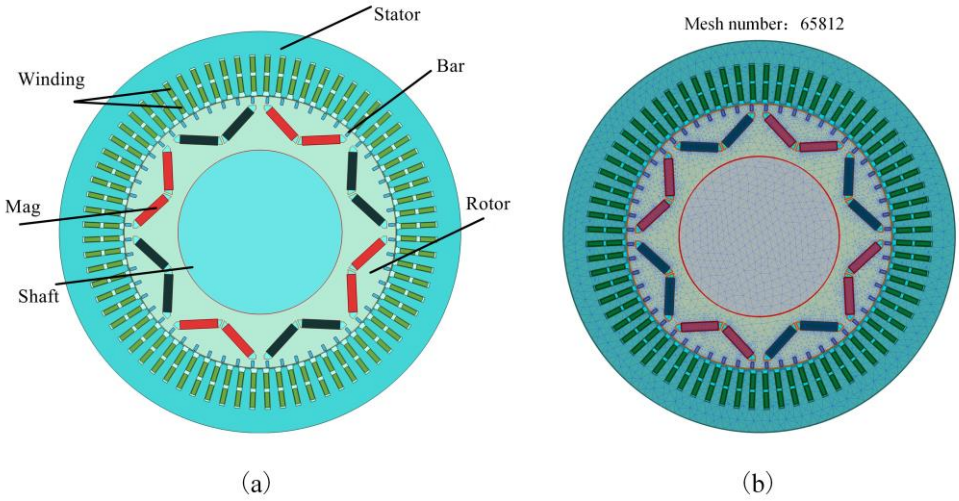

Fig. 1. Motor structure (a); subdivision (b)

To verify the accuracy of the HVLSPMSM model, a specialized experimental platform was constructed, as shown in Fig. 2. The platform includes a power analyzer, DSP data analyzer, dynamometer, AC high-voltage tester, and other professional measurement equipment. Using this platform, the actual parameters of the HVLSPMSM were measured under various conditions,

Fig. 2. Experimental platform

including no-load back electromotive force (EMF), no-load current, rated load current, and power factor. The experimental data are presented in Table 2. A comparison of the experimental data with the simulation results indicates that all deviations are within permissible error ranges. This demonstrates that the experimental data and finite element simulation results are highly consistent. This provides a solid foundation for subsequent analysis of inter-turn short circuit fault conditions.

Table 2. Data comparison

Experiment parameters (unit)	Test data	Calculated value	Variation rate (%)
EMF (kV)	5.024	5.39	7.28
No load current (A)	6.6	6.57	0.45
Rated load current (A)	38.5	38.4	0.26
Power factor	0.98	0.986	0.50

2.2. Fault state analysis

To study the HVLSPMSM under inter-turn short circuit fault conditions, an equivalent circuit was constructed to simulate the fault state. The equivalent circuit and fault model are illustrated in Fig. 3. In phase A, R_{An} and L_{An} represent the resistance and inductance of the non-short-circuited part, while R_{AC} and L_{AC} represent the equivalent resistance and inductance corresponding specifically to the k shorted coils, respectively, with R_e being the contact resistance. R_B, L_B, R_C, L_C represent the resistance ad inductance of phase B and C, respectively. The fault model and equivalent circuit are shown in Fig. 3. And in equivalent circuit, region A represents the normal three-phase circuit operation, while region B corresponds to the simulated inter-turn short-circuit fault condition. It should be noted that, although the actual stator adopts a double-layer winding structure, the equivalent circuit model simplifies each phase winding into a lumped representation, dividing it into short-circuited and non-short-circuited segments. This assumption focuses on capturing the main current and torque variations under fault conditions, without modeling the physical layering of coils.

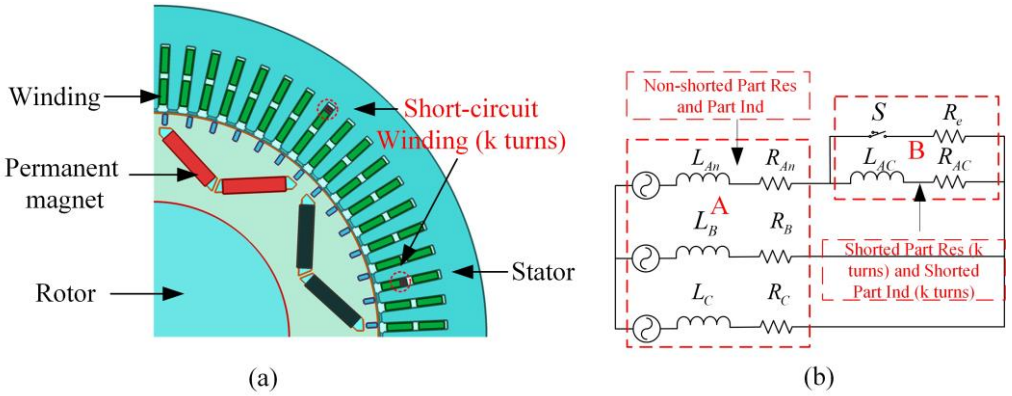

Fig. 3. Fault model (a); equivalent circuit (b)

In the simulation, the HVLSPMSM operates normally for 0.6 seconds before an inter-turn short circuit fault occurs in phase-*A* windings (with four shorted turns). The stator current and torque waveforms under normal and fault conditions is illustrated in Fig. 4. After the short circuit fault occurs, significant changes are observed in the three-phase currents, with the phase-*A* current being noticeably higher than the other two phases. Additionally, the torque shows large fluctuations with periodic variations.

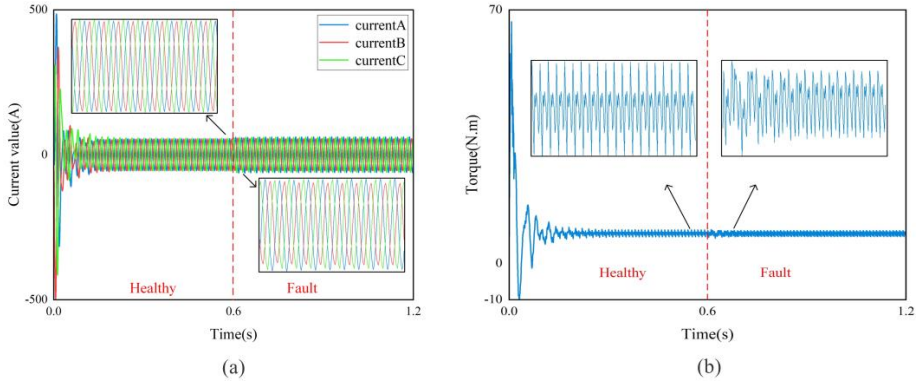

Fig. 4. Current waveform (a); torque waveform (b)

After the inter-turn short circuit, the stator current of the HVLSPMSM changes, and vibration characteristics of the motor are also affected. The output torque exhibits pulsations, which can propagate to the motor casing and induce vibrations. These torque pulsations can be used to simulate vibration intensity [15]. Therefore, in this paper, torque pulsation signals are used as a substitute for motor vibration signals for analysis.

3. IWPT-Energy gain ratio analysis principle

An ideal wavelet packet filter can accurately decompose a signal into its high-frequency and low-frequency components, with the high-frequency part containing only high-frequency signals and the low-frequency part containing only low-frequency signals. However, in practice, wavelet filters are not perfectly ideal. This results in both high-frequency and low-frequency components containing adjacent frequency band elements after decomposition. In such cases, decomposing and reconstructing the signal involves working with erroneous components from adjacent frequency bands, leading to occurrence of frequency aliasing. This is the fundamental cause of frequency aliasing.

The idea behind IWPT is to introduce two operators, C and D, based on the traditional wavelet packet decomposition and reconstruction process. In the low-frequency part, only the low-frequency signals are retained while the rest are set to zero. Similarly, in the high-frequency part, only the high-frequency signals are retained while the rest are set to zero. The implementation is carried out using FFT and inverse fast Fourier transform (IFFT) to achieve the above zeroing operation. Additionally, decimation (down-sampling) and interpolation (up-sampling) are used to correct frequency mixing phenomenon. The formulas for operators C and D are presented in Eqs. (1) to (4). In traditional wavelet packet transform (WPT), the non-ideal characteristics of the filter can

cause energy leakage between the high and low frequency branches. In improved WPT (IWPT), after decomposition, the frequency spectrum is extracted separately using FFT, retaining only the target frequency components of each frequency band, while other frequency components are set to zero. This effectively reduces the interference from cross-frequency components. The introduction of operators C and D in IWPT executes band-pass filtering functions in the low and high frequency branches, respectively, and then reconstructs the signal using IFFT. Compared to the convolution and downsampling approach in traditional WPT, this method eliminates excess frequency bands through the frequency domain windowing technique, effectively avoiding frequency aliasing phenomena.

$$C(k) = \begin{cases} \sum_{n=0}^{N_j-1} x(n)\, e^{-j\frac{2\pi}{N_j}kn}, & 0 \le k \le \frac{N_j}{4} \quad \text{or} \quad \frac{3N_j}{4} \le k \le N_j \\ 0, & \text{others} \end{cases}, \tag{1}$$

$$x_C(n) = \frac{1}{N_j} \sum_{k=0}^{N_j-1} C(k) e^{j\frac{2\pi}{N_j}kn}, \tag{2}$$

$$D(k) = \begin{cases} \sum_{n=0}^{N_j-1} x(n)\, e^{-j\frac{2\pi}{N_j}kn}, & \frac{N_j}{4} \le k \le \frac{3N_j}{4} \\ 0, & \text{others} \end{cases}, \tag{3}$$

$$x_D(n) = \frac{1}{N_j} \sum_{k=0}^{N_j-1} D(k) e^{j\frac{2\pi}{N_j}kn}. \tag{4}$$

In the equations, $n = 0, 1, \ldots, N_j - 1$; and $k = 0, 1, \ldots, N_j - 1$. N_j represents the signal length at scale $2j$, and $x(n)$ is the wavelet packet coefficient for the corresponding sub-bands at scale $2j$. $C(x)$ and $D(x)$ represent the wavelet packet node coefficients processed by the C and D operators, respectively, $x_C(n)$ and $x_D(n)$ are the signals output from IFFT after processing by $C(x)$ and $D(x)$.The process of improved wavelet packet decomposition and reconstruction can also be represented by block diagram in Fig. 5. Here, H, G, h, and g denote the convolution operations

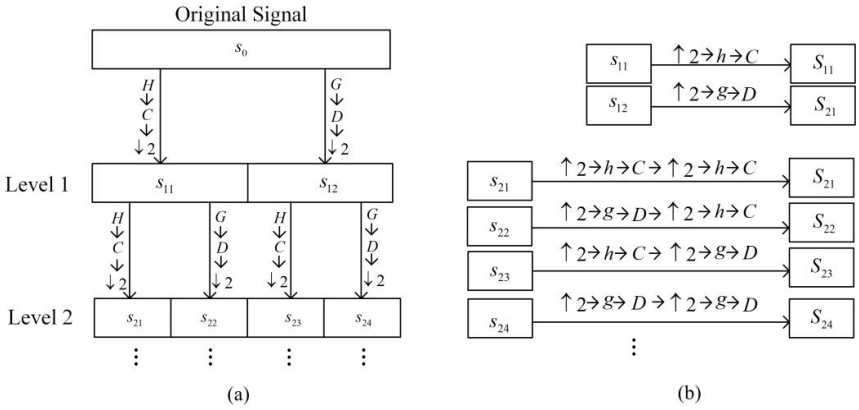

Fig. 5. Decomposition process (a); recomposition process (b)

for the low-pass and high-pass decomposition and reconstruction coefficients corresponding to the wavelet filter. $\downarrow 2$ and $\uparrow 2$ are the down-sampling and up-sampling operations, respectively. Operators C and D perform the removal of extraneous frequency components.

The workflow for extracting fault features from signals is shown in Fig. 6.

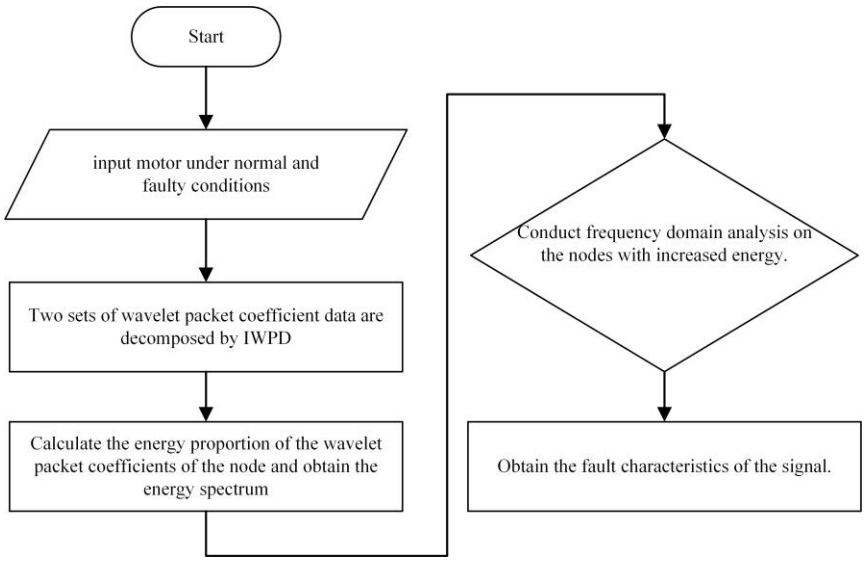

Fig. 6. Flow chart

After wavelet packet decomposition, the wavelet packet coefficients corresponding to each frequency band carry the information of the signal without altering its characteristic features, making it well-suited for feature extraction. Energy can be used to quantify the information content of the wavelet packet coefficients. If a signal is decomposed into n levels, it generates 2^n sub-bands. The energy of each sub-band can be calculated using Eq. (5). Here, E_j $(j = 0, 1, 2, \ldots, 2^n - 1)$ represents the energy of the j-th node at the level n, $X_j(n)$ represents the coefficients of the j-th node at the level n, and N is the length of the signal. Once the energy of each node is calculated, the total energy is used to compute the energy gain ratio G_j, as shown in Eq. (6). Here, $E\text{healthy}\,j$ represents the energy of the j-th node at the level n under normal conditions, and $E\text{fault}\,j$ represents the energy of the j-th node at the level n under fault conditions. If $G_j > 1$, it indicates that the fault signal energy is significantly higher than the normal signal energy, suggesting that the corresponding node is a sensitive node with fault characteristics. If $G_j < 1$, it indicates that the fault signal energy is lower than the normal signal energy, implying that the corresponding node may not be a sensitive node with fault characteristics. The formulas for E_j and G_j are presented in Eqs. (5) to (6).

$$E_j = \sum_n \left| X_j(n) \right|^2, \tag{5}$$

$$G_j = \frac{E_j^{\text{fault}}}{E_j^{\text{healthy}}}. \tag{6}$$

By comparing the energy gain ratios before and after the fault in current and torque, nodes with $G_j > 1$ can be identified. These nodes often reflect enhanced features in the corresponding frequency range. FFT is the applied to these nodes to extract and analyze the fault characteristics.

4. Result analysis

When using IWPT for analysis, it is crucial to effectively identify the characteristics and energy distribution across different frequency bands in the signal to ensure accurate decomposition and scientific analysis. The Symlet (SymN) wavelet function (where $N = 2, 3, \ldots, 10$) demonstrates good regularity and symmetry, which helps reduce distortion during signal decomposition and reconstruction. Moreover, it offers excellent frequency band division performance and accurate fault feature recognition. According to [16], inter-turn short-circuit faults in PMSMs lead to increased harmonic components, primarily odd harmonics such as the third harmonic of the fundamental frequency of the current. Reference [17] indicates that inter-turn short circuit faults induce magnetic field variations, which result in even-order harmonics in vibration signals. Based on the above findings and the Nyquist sampling theorem, this study employs the sym10 wavelet as the basis function for analysis. A sampling rate of 1100 Hz is used to analyze current and torque signals under normal conditions and three fault scenarios (short-circuit turns = $1, 4, 7$). A two-level improved wavelet packet decomposition and reconstruction are performed. The signal undergoes a two-stage decomposition, resulting in a wavelet packet tree with four terminal nodes (nodes 1–4 at the second level), and the energy gain ratio of wavelet packet coefficients for each node is calculated. Sensitive nodes are then subjected to spectral analysis to extract fault features.

4.1. Current analysis

From Table 3, it can be observed that after an inter-turn short-circuit fault occurs, the energy gain ratios of coefficient nodes 1, 2, and 3 in the current signal, following improved wavelet packet decomposition, are greater than 1. Therefore, spectral analysis was performed on these three nodes, with the results shown in Fig. 7. The frequency spectra of the three nodes under normal and varying degrees of short-circuit faults is illustrated in the figure. From Fig. 7, it can be concluded that after the fault occurs, the amplitudes of the fundamental frequency, third harmonic, fifth harmonic, and ninth harmonic all increase. Additionally, the amplitudes of the fundamental frequency, third harmonic, and ninth harmonic grow as the number of short-circuited turns increases. Although the amplitude of the fifth harmonic decreases in the case of a seven-turn short-circuit compared to a four-turn fault, it is still larger than that under normal conditions.

Table 3. Current signal G_j

G_j	Node1	Node2	Node3	Node4
Short circuit one turn	1.0268	1.0141	1.6630	0.6417
Short circuit four turns	1.1785	2.0321	1.6509	0.2759
Short circuit seven turns	1.3674	8.1823	2.0567	0.7691

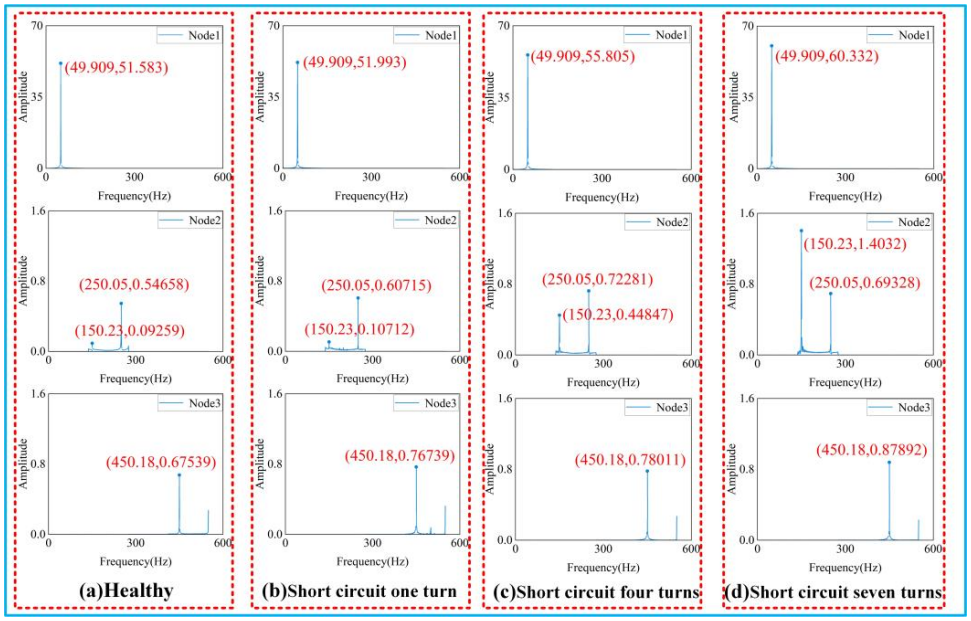

Fig. 7. Current signal analysis

The node analysis of current signal wavelet packet coefficients for a four-turn short-circuit fault using traditional wavelet packet decomposition is presented in Fig. 8. It can be observed that frequency mixing is severe across all nodes, making fault characteristics prone to interference.

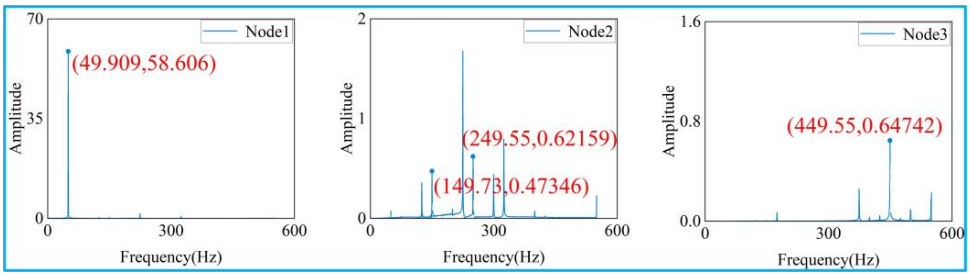

Fig. 8. Wavelet packet decomposition of current signal

This non-monotonic behavior is caused by the winding's angular asymmetry due to electrical asymmetry, and similar effects may also occur for other harmonics under different shorted-turn combinations.

4.2. Torque analysis

From Table 4, it can be observed that after an inter-turn short-circuit fault occurs, the energy gain ratios of coefficient nodes 1 and 2 in the torque signal, following improved wavelet packet decomposition, are greater than 1. Therefore, spectral analysis was performed on these two nodes, with the results shown in Fig. 9. The figure illustrates the frequency spectra of the two nodes under

normal and varying degrees of short-circuit faults. From Fig. 9, it can be concluded that after the fault occurs, the amplitudes of the second and fourth harmonics increase, and compared to normal conditions, the fundamental frequency also emerges as a new component in the fault scenario. Moreover, the amplitude of the second harmonic increases as the number of short-circuited turns grows. Although the amplitudes of the fundamental frequency and fourth harmonic do not increase consistently with the severity of the fault, they are still higher than those under normal conditions.

Table 4. Torque signal G_j

G_j	Node1	Node2	Node3	Node4
Short circuit one turn	25.3903	1.2243	0.5637	0.5370
Short circuit four turns	9.9031	1.6994	0.5042	0.6224
Short circuit seven turns	14.3375	1.1376	0.3490	0.8605

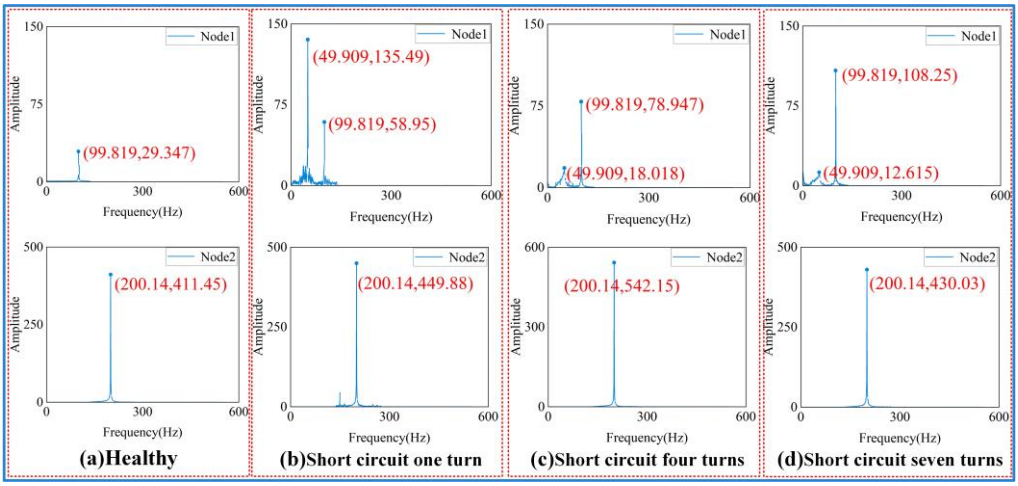

Fig. 9. Torque signal analysis

The node analysis of the torque signal wavelet packet coefficients for a four-turn short-circuit fault using traditional wavelet packet decomposition is presented in Fig. 10. It can be observed that frequency aliasing is severe across all nodes, making fault characteristics prone to interference.

The observed increases in the fundamental, 2nd, and 4th harmonic components in the torque spectrum provide valuable indicators for inter-turn short circuit faults. It should be noted that external power supply asymmetry (e.g., unbalanced three-phase voltages) can also induce qualitatively similar effects in the torque spectrum, such as increased fundamental and even-order harmonic amplitudes. However, the distinctive signature identified concurrently in the stator current signal – namely the significant increase in the 3rd and 9th harmonics – serves as a key discriminator. The combined utilization of features from both torque and current signals in the proposed method enhances diagnostic specificity against such potential confounding factors.

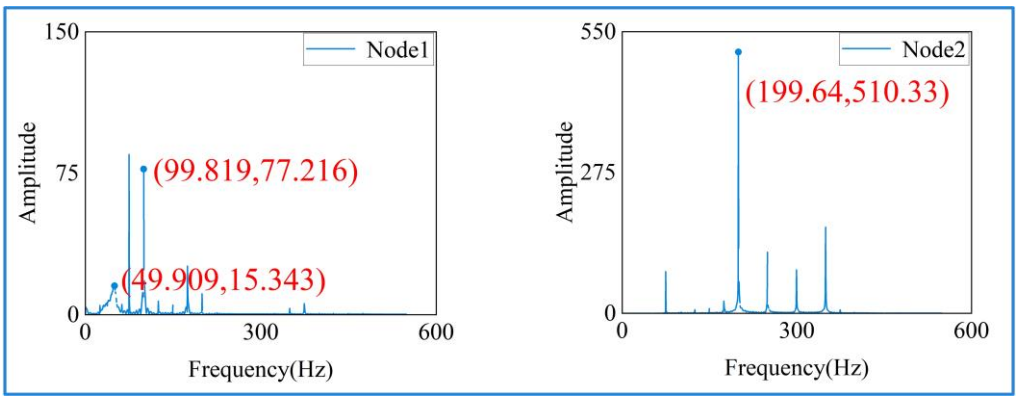

Fig. 10. Wavelet packet decomposition of torque signal

5. Conclusion

To address the precise identification of inter-turn short-circuit faults in HVLSPMSMs, this paper investigated the frequency domain characteristics of current and vibration under inter-turn short-circuit conditions and proposed an improved wavelet packet algorithm combined with energy gain ratios. The results indicate:

1. Traditional wavelet packet decomposition suffers from frequency alising, and the conventional energy analysis method of wavelet packet coefficients fails to accurately reflect energy variations. In contrast, the improved wavelet packet analysis algorithm not only effectively eliminates frequency alising, but also when combined with energy gain ratio analysis, accurately reveals energy changes before and after faults, enabling precise fault feature analysis without interference from unrelated harmonics.
2. Under inter-turn short circuit fault conditions, the amplitude of current signal components at f, $3f$, $5f$, and $9f$ significantly increases. Similarly, the fundamental frequency and $2f$ components of vibration signal also increase. These are the main frequency-domain characteristic frequencies for identifying inter-turn short-circuit faults.
3. This study analyzed a specific fault – inter-turn short-circuit fault – in a high-voltage self-starting permanent magnet synchronous motor and examined varying levels of fault severity. The proposed method effectively identifies inter-turn short-circuit fault features. However, its effectiveness in detecting different fault types or faults at different locations requires further investigation, and this will be the focus of future research.
4. It is worth noting that due to the high voltage and high-power characteristics of the HVLSPMSM, this study was unable to obtain experimental data in a fault state under actual operating conditions, and the fault analysis still relies on the simulation model. Future research will consider introducing fault injection mechanisms and improved high-voltage testing platforms to enhance the adaptability and reliability of the method under actual operating conditions.

Acknowledgements

This work was sponsored in part by the National Natural Science Foundation of China under Grant 52177063,in part by Natural Science Foundation of Henan under Grant 232300421070, in part by the National Natural Science Foundation of China under Grant 52477066, and in part by the Program for Science & Technology Innovation Talents in Universities of Henan Province under Grant 23HASTIT026, and in part by the Science and technology project of Henan Province under Grant 232102220080, 222102320074, 242102221002.

References

[1] Lyskawinski W., *Comparative analysis of energy performance of squirrel cage induction motor, line-start synchronous reluctance and permanent magnet motors employing the same stator design*, Archives of Electrical Engineering, vol. 69, no. 4, pp. 967–981 (2020), DOI: 10.24425/aee.2020.134642.

[2] Yang C.X., Wang Y.M., Qiu H.B., *Study on the influence of three-phase voltage unbalance on electromagnetic performance and vibration of high-voltage line-start permanent magnet synchronous motor*, Archives of Electrical Engineering, vol. 74, no. 42, pp. 209–226 (2025), DOI: 10.24425/aee.2025.153020.

[3] Luo P., Yin Z., Zhang Z., Zhang Y., Zhang P., Liu J., *Diversified Diagnosis Strategy for PMSM Inter-Turn Short-Circuit Fault via Novel Sliding Mode Observer*, IEEE Transactions on Power Electronics, vol. 39, no. 4, pp. 4149–4159 (2024), DOI: 10.1109/TPEL.2024.3352077.

[4] Li H., Shi T., *Diagnosis of Inter-Turn Short-Circuit Incipient Fault in Permanent Magnet Synchronous Motors Using Input Current on the Power Side*, IEEE Transactions on Industrial Informatics, vol. 20, no. 12, pp. 13741–13752 (2024), DOI: 10.1109/TII.2024.3431632.

[5] Zhang Y., Liu G., Zhao W., Zhou H., Chen Q., Wei M., *Online Diagnosis of Slight Interturn Short-Circuit Fault for a Low-Speed Permanent Magnet Synchronous Motor*, IEEE Transactions on Transportation Electrification, vol. 7, no. 1, pp. 104–113 (2021), DOI: 10.1109/TTE.2020.2991271.

[6] Kao I.-H., Wang W.-J., Lai Y.-H., Perng J.-W., *Analysis of Permanent Magnet Synchronous Motor Fault Diagnosis Based on Learning*, IEEE Transactions on Instrumentation and Measurement, vol. 68, no. 2, pp. 310–324 (2019), DOI: 10.1109/TIM.2018.2847800.

[7] Głowacz Z., *Automatic recognition of armature current of Dc Motor with application of FFT and GSDM*, Archives of Metallurgy and Materials, vol. 56, no. 1, pp. 25–30 (2011), DOI: 10.2478/v10172-011-0003-2.

[8] Lale T., Gümüs B., *A New Approach based on Electromechanical Torque for Detection of Inter-Turn Fault in Permanent Magnet Synchronous Motor*, Electric Power Components and Systems, vol. 49, no. 1, pp. 1–13 (2022), DOI: 10.1080/15325008.2022.2133193.

[9] Heydarzadeh M., Zafarani M., Akin B., Nourani M., *Automatic fault diagnosis in PMSM using adaptive filtering and wavelet transform*, 2017 IEEE International Electric Machines and Drives Conference (IEMDC), Miami, USA, pp. 1–7 (2017), DOI: 10.1109/IEMDC.2017.8002381.

[10] Rosero J., Espinosa A.G., Cusido J., Ortega J.A., Romeral L., *Simulation and Fault Detection of Short Circuit Winding in a Permanent Magnet Synchronous Machine (PMSM) by means of Fourier and Wavelet Transform*, 2008 IEEE Instrumentation and Measurement Technology Conference, Victoria, Canada, pp. 411–416 (2008), DOI: 10.1109/IMTC.2008.4547070.

[11] Damnjanovic D., Ciric D., Peric Z., *Wavelet-based audio features of DC motor sound*, Facta Universitatis-Series Electronics and Energetics, vol. 34, no. 1, pp. 71–88 (2021), DOI: 10.2298/FUEE2101071D.

[12] Gangsar P., Tiwari R., *Multifault Diagnosis of Induction Motor at Intermediate Operating Conditions Using Wavelet Packet Transform and Support Vector Machine*, Journal of Dynamic Systems Measurement and Control-Transactions of the Asme, vol. 140, no. 8, pp. 1472–1483 (2018), DOI: 10.1115/1.4039204.

[13] Pietrowski W., Górny K., *Detection of inter-turn short-circuit at start-up of induction machine based on torque analysis*, Open Physics, vol. 15, no. 1, pp. 851–856 (2017), DOI: 10.1515/phys-2017-0101.

[14] Xia Y.-K., Li X.-Y., *Calculation and Experiment of Stray Inductance of PCB Double-Pulse Test Circuit Based on Three-Dimensional Simulation*, IEEE Access, vol. 10, pp. 58769–58776 (2022), DOI: 10.1109/ACCESS.2022.3179662.

[15] Xia Y.K., Li X.Y., Luo Y.J., *Inter-Turn Short Circuit Fault Detection of PMSM Based on Wavelet Packet Energy Spectrum and CEEMDAN-HT*, Journal of Electrical Engineering & Technology, vol. 19, no. 3, pp. 1379–1393 (2024), DOI: 10.1007/s42835-023-01597-7.

[16] Wang X.Y. *et al*., *Analysis of Harmonic Current in Permanent Magnet Synchronous Motor and Its Effect on Motor Torque*, Journal of Electromagnetic Analysis and Applications, vol. 4, no. 1, pp. 15–20 (2012), DOI: 10.4236/jemaa.2012.41003.

[17] Yang G.L. *et al*., *The influence of ITSF on vibration of high voltage Line-Start permanent magnet synchronous motor*, Compel-the International Journal for Computation and Mathematics in Electrical and Electronic Engineering, vol. 43, no. 2, pp. 301–317 (2024), DOI: 10.1108/compel-11-2023-0610.